Structures 57 (2023) 105132

Contents lists available at ScienceDirect

Structures

journal homepage: www.elsevier.com/locate/structures

Experimental and numerical simulation of pull-out response in textile-reinforced concrete

S.G. Venigalla, A.B. Nabilah *, N.A. Mohd Nasir, N.A. Safiee, F.N.A. Abd Aziz

Department of Civil Engineering, Universiti Putra Malaysia, 43400 Serdang, Selangor, Malaysia

ARTICLE INFO

Keywords:
Textile reinforced concrete
Finite element analysis
Carbon fibre
Bond-slip relation
Pullout test

ABSTRACT

Textile-reinforced concrete (TRC) is a construction material that uses continuous fibres such as carbon to create a lightweight and durable structural system. Even though TRC possesses vast possibilities in terms of its usage, identification of bond-slip behaviour at the material interface is one of the limitations that need to be addressed. Based on the literature, there are difficulties in determining the bond-slip relationship both experimentally and numerically, creating inconsistency in the results. This study aims to determine the bond-slip relation of TRC through pullout tests and validated through finite element analysis to replicate the actual bond-slip behaviour at the interface. The bond characteristics of TRC were assessed using a double-sided pullout test setup with different bond lengths of textile, namely 20 mm, 30 mm, 40 mm, 50 mm, and 60 mm. It was noticed that in short bond specimens (20 mm, 30 mm, and 40 mm), the phenomena of pullout failure were due to weakened bond at the interface until pre-peak, followed by complete loss of adhesive bond due to debonding of fibre. However, for the specimens with longer bond lengths (50 mm and 60 mm), rupture of the textile leading to a sudden loss of bond capacity was observed. Additionally, the general fibre pullout phenomenon curve was used to explain the debonding process. Using a calibrated tri-linear bond-slip interface relation, the numerical model was developed to simulate the pull-out response of fibre. The numerical model was able to reproduce experimental results, including maximum load, post-peak behaviour, and interfacial slip. The difference of maximum shear stress between pull-out tests and numerical modelling was within 2 % while the slip difference was between 4 and 31 % for different bond lengths. However, for longer bond lengths, the fibre failure mode was due to pullout instead of rupture, unlike the experimental results.

1. Introduction

The use of precast elements in the construction field is increased to expedite the construction time and reduce costs. There are many techniques evolved to substitute conventional construction methods, such as using lightweight concrete by replacing existing reinforcement materials with short and continuous fibres, which produce durable and slender elements. However, the drawback of using short fibres is their unsystematic distribution, which results in segregation and reduces the elements' effectiveness [17]. To subdue this effect, the use of continuous fibres as reinforcement, creating textile-reinforced concrete, evolved in the present decade [6].

Textile-reinforced concrete (TRC) is a relatively new composite material composed of fine-grained cement-based mortar layered with textile fibres as the mesh (Fig. 1). TRC is widely used to retrofit existing structures as well as for aesthetic purposes [20]. As of now, using TRC in conventional construction is still a constraint because of the limitation in the bending capacity and the improper theory to explain the bond-slip behaviour at the textile-concrete interface. Given these limitations, research and collaborative works were carried out over a decade in Europe and Asia on TRC. The major studies are mostly focused on evaluating the structural properties of TRC, such as bending and tension capacities [11,19,25]. The tested specimens were fabricated in the form of plates subjected to tension or bending. The majority of results from various studies depended on the textile type, pattern, aspect ratio, and mortar mix. It was also noticed from past studies that in TRC elements, the interfacial bond-slip behaviour of textile fibre in concrete plays a prominent role that influences global structural behaviour [26]. Unlike conventional reinforcements, textile is weak in bending due to their size and are difficult to curtail. These factors were majorly influenced by the bond-slip relation as it is the critical input parameter for numerical

* Corresponding author.
E-mail addresses: gs54602@student.upm.edu.my (S.G. Venigalla), nabilah@upm.edu.my (A.B. Nabilah), nazline@upm.edu.my (N.A. Mohd Nasir), norazizi@upm.edu.my (N.A. Safiee), farah@upm.edu.my (F.N.A. Abd Aziz).

https://doi.org/10.1016/j.istruc.2023.105132
Received 20 April 2023; Received in revised form 19 July 2023; Accepted 24 August 2023
Available online 2 September 2023

Nomenclature

σ	Stress
ε	Strain
f_{cr}	Compressive strength of mortar mix
f_t	Tensile strength of mortar mix
G_c	Fracture energy of mortar mix
E_c	Elastic modulus of mortar
E_f	Elastic modulus of textile
ε_c	Compressive strain at maximum stress
ε_u	Ultimate compressive strain
ε_t	tensile strain at maximum stress
ε_{tu}	Ultimate tensile strain
f_f	Tensile strength of textile fibre
υ	Poisson's ratio of mortar
t_i	Thickness of interface
ε_f	The tensile strain of textile fibre
u	Displacement
u_o	Slip at friction phase
u_{max}	Slip at peak load
P_E	Pull-out load at the end of the elastic phase.
P_{max}	Pull-out peak load
P_o	Pull-out load at friction phase
k_1	The ratio of maximum stress to peak load displacement
k_2	The ratio of shear stress at the friction phase and shear stress at peak load
$\tau(u)$	Shear stress at displacement 'u'
τ_o	Shear stress at the friction phase
τ_{max}	Shear stress at peak load
K_{nn}	Normal stiffness modulus
K_{tt}	Shear stiffness modulus

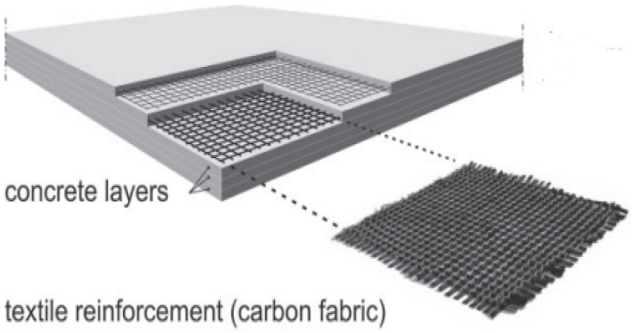

Fig. 1. Textile-reinforced concrete [21].

models to showcase the structural response of TRC [22].

To determine the bond-slip mechanism, fibre pullout test methods were developed. In practice, one-sided and two-sided pullout tests were used for TRC plates. The one-sided pullout tests on TRC were similar to conventional tests conducted on steel bars. A group of textile yarns were bundled in the epoxy block at one end and the other end was placed inside a concrete block. Similar to conventional concrete, the pullout tests were carried out on unmanufactured single yarn where the obtained results do not replicate a single fibre pullout as the fibre fails due to breaking. To avoid the breaking phenomena, double-sided pullouts tests were developed by researchers with an unsymmetrical clamping length [12,13,15,24,29]. The pullout load versus displacement results were determined using two-sided notches. However, due to the unsymmetrical clamping lengths, the shorter bond lengths of the textile cannot be tested effectively. Therefore, to test fibre capacity for shorter lengths, Williams Portal et al., [27] performed pullout tests on TRC with symmetrical clamping lengths. Further, many test setups with direct and indirect clamping to the testing machine and samples with cross-sections like dog-bone shape and *T*-shape were also developed [10]. All the test methods were developed based on conventional methods considering standard cross-section dimensions, mesh size, and rate of loading. However, to assess the bond strength, the textile must be ensured to fail due to pullout.

From the test results, only the physical behaviour of the textile such as pullout capacity and the type of failure can be obtained, whereas, the non-linear bond-slip behaviour at the textile-mortar interface cannot be determined. To explain the non-linear behaviour at the interface, various numerical methods were developed. In these methods, the materials are considered to behave as linearly elastic until failure, and the interface was modelled with embedded textiles using cohesive interface models. To simulate the bond-slip response, the textile should be modelled with a bond-slip element at the interface, with the non-linear interface curves given as the input. For fibre-reinforced polymer, numerous bond-slip models were developed to explain FRP-mortar interface behaviour. The models were classified as (i) linear descending, where the elastic stage is not considered, (ii) bi-linear, a two-stage shear stress-slip curve with a non-linear stage, (iii) tri-linear, similar to bilinear with friction stage, (iv) two-stage ascending non-linear, where power function is used in the ascending branch, and (v) Borchert law, modified compared to all models suppressing the original bond shear plateau [9]. Similar to FRP, the five main bond-slip models are used to model the interfacial behaviour of textile-reinforced concrete (TRC). The selection of a bond-slip model depends on the characteristics of the materials, and the pull-out response of the specific TRC system.

The present study aims to explain the complex bond behaviour in TRC for different embedded lengths through experimental and numerical analysis. The embedded lengths were varied to assess the bond capacity and the fibre failure pattern. Initially, a suitable mortar mix for TRC was designed and the strength properties of conventional mortar specimens were determined. The double-sided pull-out tests with equal clamping lengths for a single fibre were tested and the bond failure phenomena were examined using the fibre delamination process. Further, a numerical method was developed to explain the bond-slip phenomena at a micro level using a tri-linear bond-slip to model the interface failure. Finally, the experiment results were compared with finite element analysis and validated.

This research discusses the fibre pullout phenomenon at different stages and provides a general simplification of bond-slip modelling using tri-linear bond-slip law. The model was validated through experimental work and numerical analysis. The outcome will be useful in predicting the response of TRC under loads, allowing for its widespread use in the industry.

2. Experimental study

2.1. Materials

In this work, cement-based fine-grained concrete was used, with a maximum aggregate size of 1.18 mm based on Yin et al. [28] and Shiping et al. [23]. The mortar mix is selected based on trails with micro silica percentage as constant with varying fly ash, cement, and water-binder ratios. The final mix comprises 68.5 % Type-I ordinary Portland cement-42.5 N grade, 25 % of fly ash, and micro silica fume of 6.5 % with a water-binder (w/b) ratio of 0.35. A naphthalene sulfonate

(Darex Super 20) based admixture was also used to produce a flowable concrete. To choose a suitable w/b ratio, flow tests were performed according to ASTM C230/C230M-08 [2]. The mortar mix proportion details are tabulated in Table 1. The mortar strength was tested under compression for specimens of size 50 mm × 50 mm × 50 mm according to BS EN 1015-11 [5]. The mean compressive strength and modulus of elasticity of the mortar mix after curing for 28 days were 47 MPa and 35 GPa respectively with a mortar flow of 15.5 cm.

In this study, a commercially available carbon fibre mesh with multi-filament yarns was used as the textile reinforcement, as carbon fibre is durable and also has high strength. The textile fibre has a mesh spacing of 5 mm × 5 mm with a density of 1.79 g/cm^3. Each yarn comprises of 12 k filaments in the two orthogonal directions. The properties of the textile are indexed in Table 2. The textile yarns were further stretched and coated with bisphenol-based epoxy (EPIKOTE Resin 828) and polyamide resin 651 hardener at a ratio of 5:2, to avoid tensile weakening and mortar penetration through filaments. The coated textile was cured at 25 °C for 48 h [14] (see Fig. 2).

2.2. Bond characterization tests

The bond strength of textile-reinforced concrete is usually determined by experimental testing of TRC plates under tension. In general, the bond-slip of conventional rebar in concrete can be determined by a direct pullout test, based on ASTM 234-91 (2000). For TRC, the conventional pullout test setup cannot be used due to the limitation of fibre diameter, which leads to rupture. In this process, many experimental techniques and studies were evolved to determine bond slip in TRC. Initially, Banholzer, [3] adopted a direct pullout test similar to ASTM 234-91 (2000), where one end of the fibre is placed in the mortar and the other end in an epoxy block with testing and gripping lengths of 50 mm and 30 mm respectively. The results obtained were unable to resemble the intended bond-slip behaviour, due to the premature yielding of fibre prior to the ultimate load. To avoid this phenomenon, Butler (2009) and Lorenz and Ortlepp [15] developed a textile pullout test method with two-sided notch and unsymmetrical clamp lengths. This is to overcome yielding and also to introduce direct force on the textile fibre in the concrete matrix. Further, Williams Portal et al., [27] and Jiang et al., [10] developed a pullout test method where the fibre can also be tested with desired bond lengths and also with equal clamping lengths, to minimize the effect of gripping.

In the present study, the textile was tested with a double-sided pullout with notches and equal clamping lengths. The dimension of the pullout specimen and testing method was designed according to the RILEM TC 232-TDT [4] and AC434 [1] recommendations. The TRC specimens were cast as rectangular cross-sections with a dimension of 300 mm × 50 mm × 12 mm. The cement mortar is placed in two halves, first, a 6 mm layer of mortar was poured, and coated carbon textile was placed and fastened by a formwork, followed by placing the second layer of mortar. The pullout specimens were removed from formwork after 24 h and water cured for 28 days. Finally, on the day of testing, uneven concrete edges were trimmed and the specimen cross-section was inspected at various points with an accuracy of 0.2 mm. Only a single fibre was tested by making an appropriate notch on the plate (see Fig. 2). Five different bond lengths, ranging between 20 mm and 60 mm (with an interval of 10 mm) were chosen to identify the failure pattern of the textile. The bond lengths were limited by making a saw cut underneath the clamping length of 50 mm (see Fig. 3). The tests were performed on 3 samples for each bond length, to obtain the average pullout trend.

Table 1
Mortar mix proportions.

Cement (kg/m^3)	Fly ash (kg/m^3)	Micro silica (kg/m^3)	Fine aggregate (kg/m^3)		Water (kg/m^3)	Superplasticizer
			0–0.6 mm	0.6–1.18 mm		
583.0	212.8	55.31	390.1	791.9	297.9	0.8 % of binder

Table 2
Carbon textile properties.

Property	Units	Value
Each Yarn	Nos	12,000 filaments
Mesh size (0°/90°)	mm × mm	5 × 5
Tensile Strength	GPa	4.5
Elastic Modulus	GPa	230
Density	g/cm^3	1.79
Diameter	μm	7
Elongation	%	1.9

The tests were carried out on a displacement-controlled universal testing machine with a capacity of 10 kN (see Fig. 3). The specimens were clamped on either side using steel box sections of size 50 mm × 20 mm at both ends to transfer load. Further, the entire plate setup was clamped directly to the machine through 60 mm × 35 mm box sections at the top and bottom supports. The actual displacement of the TRC plates was identified by a crack-opening relation at a loading rate of 1 mm/min. The crack-opening phenomenon was measured using an extensometer with a maximum gauge length of 50 mm, which was directly connected to the machine. The pullout load and displacements were recorded every second and continued until specimen failure.

2.3. Experimental results

To explain the pullout process, a general fibre pullout phenomenon curve was used (see Fig. 4). The failure pattern was divided into three stages, namely elastic, damage, and friction. The elastic stage (stage A) is attributed to the initial loading phase, where the composite behaviour of the materials is considered as perfectly elastic. During this phase, the fibre and surrounding mortar deform elastically with linear stress–strain behaviour. The material properties such as elastic modulus describe the stiffness of the material and Poisson's ratio represents the lateral response with respect to axial deformation. Beyond the elastic stage (P_E), the damage (stage B) initiates at the interface where the fibre starts debonding. In this stage, the peak load (P_{max}) will be reached from the contribution of interfacial friction force in the debonded length. As the undamaged (bonded) length becomes too short, the pullout force starts to decrease. At the end of stage B, it is considered that the fibre will be debonded completely at the matrix interface, and the load–displacement response will be parabolic. Finally in stage C, debonding becomes unstable and the pullout force starts to drop instantly due to sliding phenomena. Thus, the whole embedded length starts to slide from the mortar matrix.

The pullout force vs displacement results of TRC plates for bond lengths of 20 mm, 30 mm, 40 mm, 50 mm, and 60 mm are described in Fig. 5. From the experimental results, the linear elastic behaviour of the pullout curve was observed initially for all the bond lengths. The slope of the load–displacement curve in the elastic range was similar for all samples, except for the 30 mm bond length which shows a stiffer behaviour. The possible reason was due to the restraining forces exerted at the textile interface which was greater than the driving pullout force. When fibre starts losing its linear elastic property at the interface, the interfacial frictional force in the debonded length was added to the force that helps to achieve the maximum load (P_{max}). In addition, the peak load generally increased with increasing bond length, due to the larger surface area surrounding the textile to transfer the shear stress to the concrete.

The average maximum pullout forces corresponding to 20 mm, 30 mm, 40 mm, 50 mm, and 60 mm bond lengths were recorded as 724 N, 876 N, 926 N, 1126 N, and 1305 N respectively. Similarly, the displacements recorded at peak loads were 0.28 mm, 0.16 mm, 0.42 mm, 0.55 mm, and 0.80 mm for the corresponding bond lengths. Beyond the peak load (P_{max}), a significant drop in load was observed for all the bond

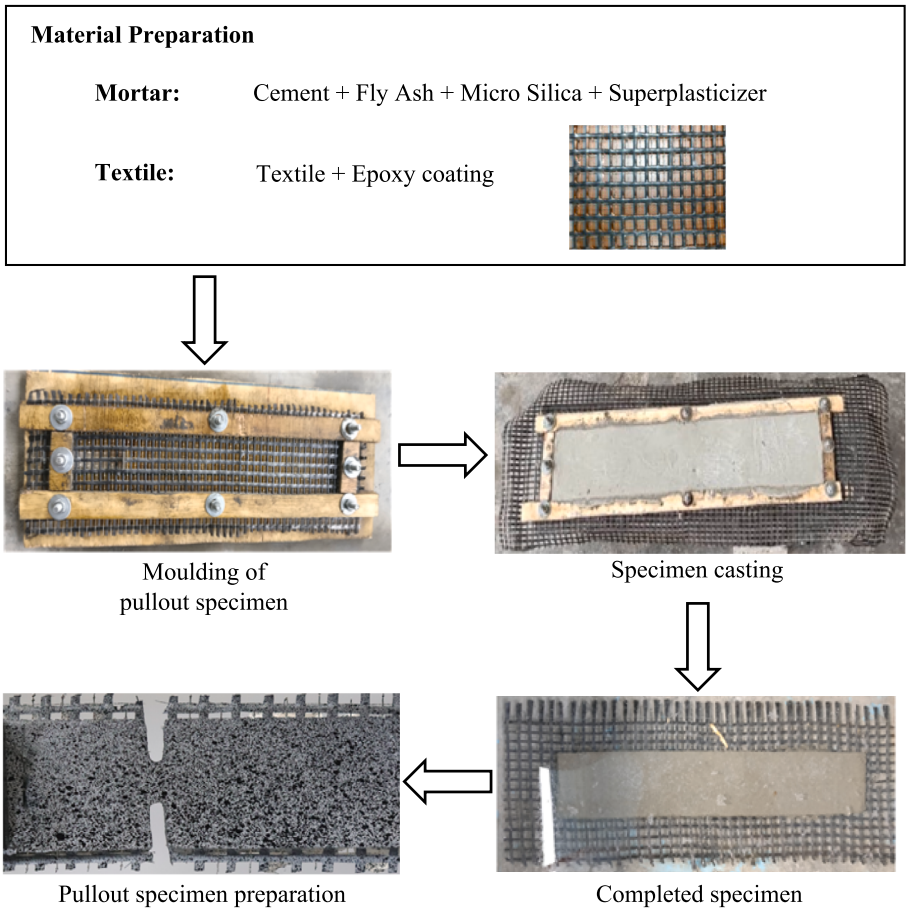

Fig. 2. TRC plate fabrication process flow diagram.

lengths. This phenomenon was due to the increase in debonding length of the fibre from the interface, as shown in Fig. 4. Samples with shorter bond lengths (20 mm to 40 mm) have prolonged drop in load after reaching the peak strength due to pullout failure of the fibre. Comparatively, the decrease in load after the maximum capacity for samples with longer bond lengths (50 mm and 60 mm) was sudden due to rupture failure. The loading was continued until complete fibre debonding. Finally, once the fibre debonded completely from the mortar interface, the cracking pattern was substantial at the notch and sliding of fibre from the shorter length was observed in all the specimens. At this stage, for shorter bond lengths, the force versus displacement was controlled up to an extent by the residual strength at the interface and also by frictional forces. Whereas, for longer bond lengths, only frictional forces were responsible for resisting the load, hence the failure was instantaneous. Also from the tests, it was noticed that beyond the full debonding point, the force–displacement curve was non-linear for all the bond lengths.

The failure pattern of tested samples for different bond lengths is shown in Fig. 6. It was noticed that the specimens with bond lengths of 20 mm, 30 mm, and 40 mm failed due to pullout failure of the textile (Fig. 6(a)–(c)), whereas rupture was the cause of failure in the 50 mm and 60 mm bond length specimens (Fig. 6(d) and (e)). In the case of short bond length specimens (20 mm to 40 mm), the phenomena of pullout failure were due to weakened bond at the interface until pre-peak, followed by complete loss of adhesive bond due to debonding of fibre. Finally, the leftover pullout force was dependent on friction between the fibre and concrete. However, for the specimens with long bond lengths (50 mm and 60 mm), rupture of the textile which leads to sudden loss of strength was observed.

2.4. Comparisons with literature

In this section, the current pullout responses of textile fibre for shorter bond lengths were compared with three other works reported in the literature, as shown in Table 3. As discussed in Section 1, the pullout behaviour is highly dependent on the material characteristics and testing methods. Williams Portal et al. [27] examined the bond behaviour of TRC with carbon textiles of mesh size 30 mm × 30 mm with a bond length of 25 mm. The results indicated a strong bond between reinforcement and mortar matrix compared with other works, where the slip recorded at peak load was 0.10 mm. However, comparatively higher pullout capacity was attained in this study due to the mesh size and epoxy coating that protects the deterioration of the textile.

The effect of uncoated textiles can be compared to the study reported by Zhu et al. [30]. The uncoated fibre resulted in the failure of 30 percent of the filaments before reaching the maximum load due to the impregnation of mortar in the fibre, causing a drop in the pullout capacity of the fibre. This, coupled with a low rate of loading (0.2 mm/min) causes the extended fibre damage and debonding phases. Hence, the pullout response of fibre exhibited a linear ascending branch up to the maximum load with a larger slip followed by a softening post-peak behaviour with a slow descending portion. The effect of asymmetrical clamping can be compared to the study by Lorenz et al. [16]. Even though a similar failure pattern was noticed, the pullout capacity was comparatively lower than in the other studies. The pre and post-peak behaviour were almost linear without the softening branch. However, the relative displacement of fibre was also high. Subsequently, the non-symmetric mesh pattern will affect the bond capacity, resulting in a weaker pullout capacity with a larger slip. Even though the testing methods and material configurations were contrasting, the failure

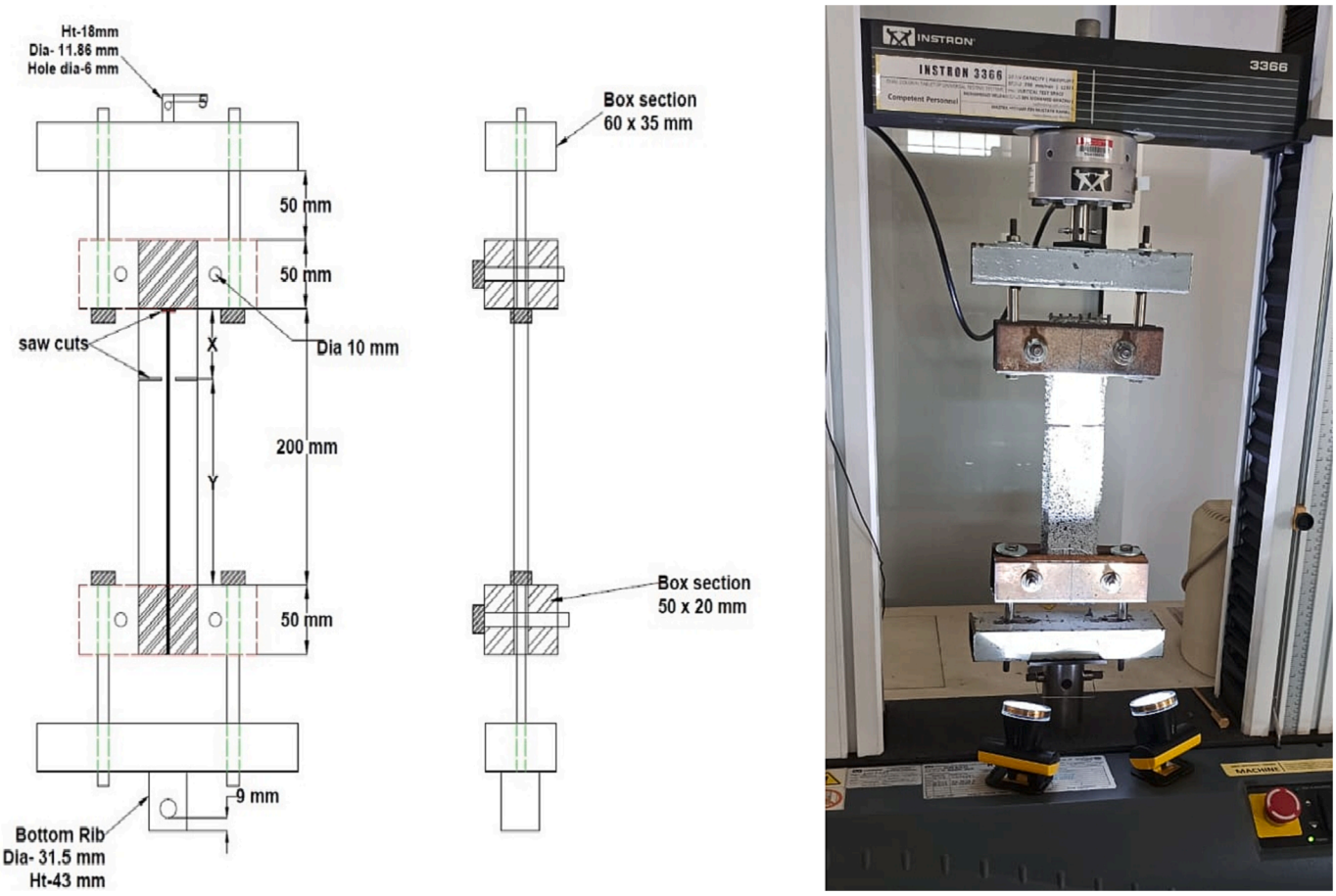

Fig. 3. Testing of TRC plate.

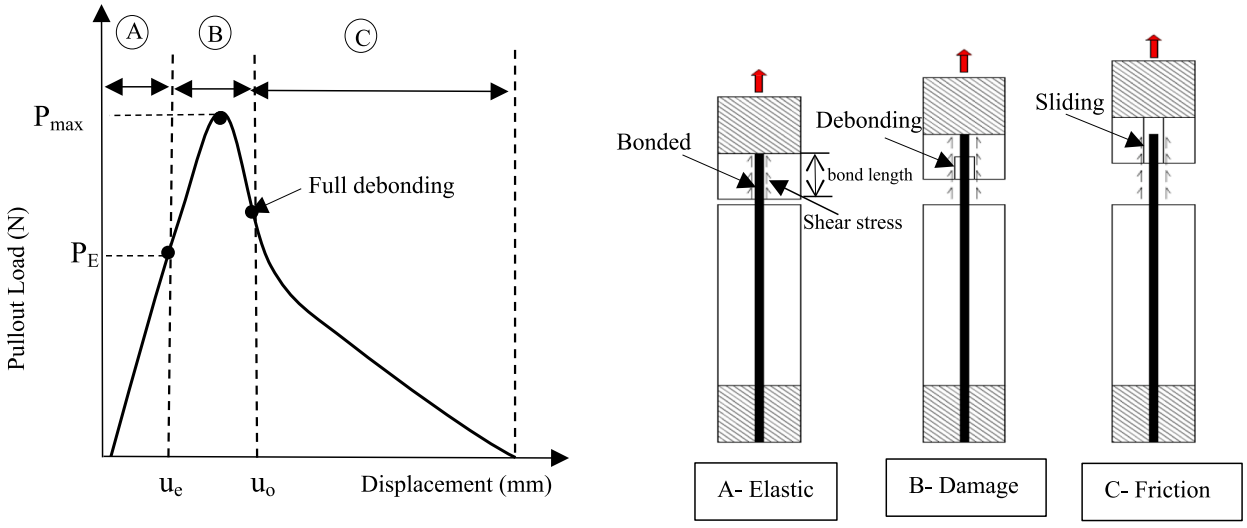

Fig. 4. Fibre pullout phenomenon.

pattern was similar and fibre pullout phenomena were continued with elastic, damage, and friction stages. Comparatively, the damage phase was prolonged for symmetrical clamping lengths due to evenly distributed stress along the bond length, whereas for unsymmetric clamps, the damage is instantaneous due to stress concentration and friction stage was prolonged due to the fibre failure.

3. Finite element modelling

In the present study, Diana FEA 10.5 software was used to determine the bond-slip behaviour in textile-reinforced concrete. A 3D non-linear approach was used to visualize the debonding process at the textile-mortar interface. The specimens with multiple bond lengths from 20 mm to 60 mm were modelled with similar dimensions replicating experimentally tested specimens. Further, developed bond-slip curves

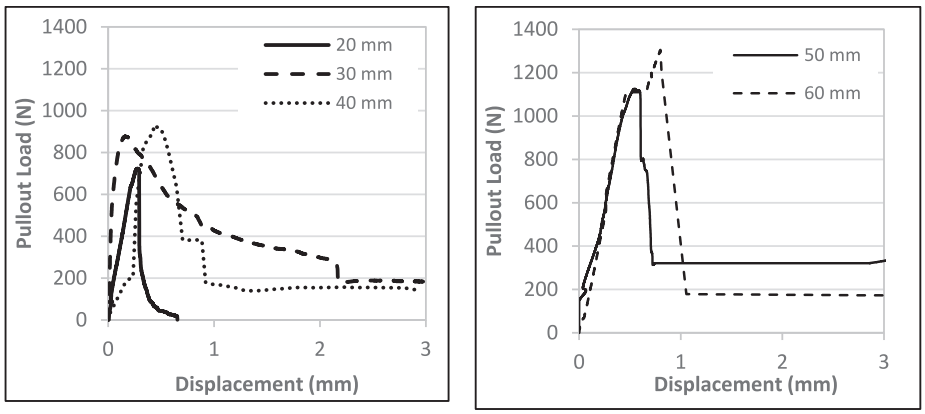

(a) (b)

Fig. 5. Pullout load versus displacement curves for bond lengths of (a) 20 to 40 mm, and (b) 50 and 60 mm.

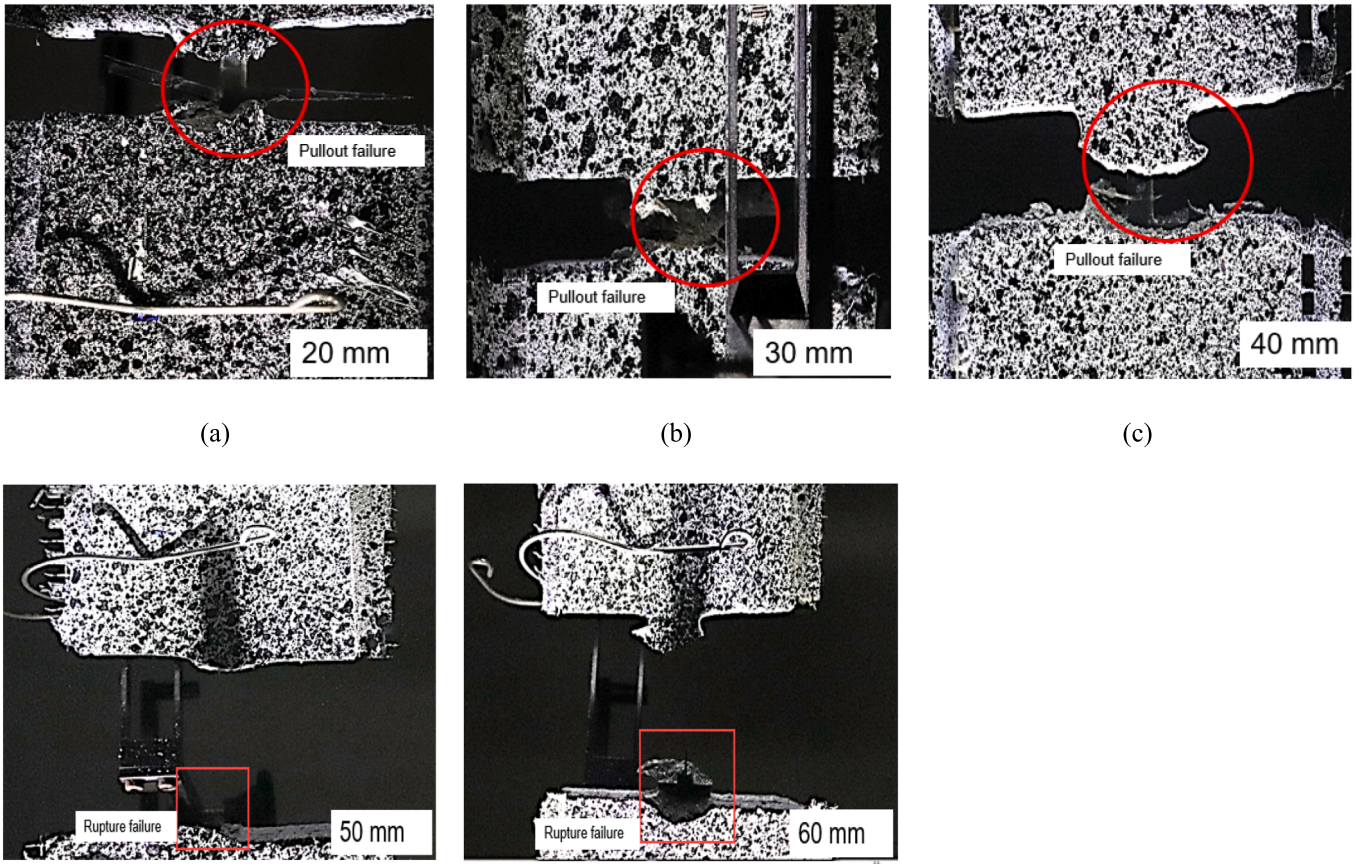

(a) (b) (c)

(d) (e)

Fig. 6. Fibre failure pattern for bond lengths of (a) 20 mm, (b) 30 mm, (c) 40 mm, (d) 50 mm, and (e) 60 mm.

were considered to model the interface. Finally, the finite element analysis was compared to the experimental results to evaluate the accuracy of the model.

3.1. Element and material properties

TRC is a composite of two main materials, namely mortar and textile. The mortar was modelled as 4-noded TE12L solid plates and the textile as a 2-noded L4TRU truss element. The textile cross-section was assigned as circular and continuous in interfaces.

The mortar was modelled using the total strain-based crack model with inelastic stress–strain behaviour in tension and compression zones. For compressive behaviour, the uniaxial parabolic stress–strain curve was adopted considering fracture energy and rotating crack orientation [18]. For the tensile behaviour of mortar, a uniaxial bilinear curve was used (Fig. 7(a)). The property of the carbon textile was assigned as linear-elastic as the failure of concrete happens before the textile (Fig. 7 (b)). The material properties assigned in the model are summarized in

Table 3
Pullout results comparison with existing studies.

Reference	Textile type	Mesh size (mm × mm)	f_{cr} (MPa)	E_f (GPa)	Bond length (mm)	Max. pullout load (N)	Slip at peak load (mm)	Failure type
Present study	Carbon with epoxy	5 × 5	47	230	20	724	0.275	Pullout
Zhu et al. [30]	Carbon	6.49 × 5	74.1	181	30	225	0.20	Pullout
Williams Portal et al. [27]	Carbon	30 × 30	53.6	230	25	629	0.10	Pullout
Lorenz et al. [16]	Carbon with epoxy	7.2 × 18	–	205	20	220	0.19	Pullout

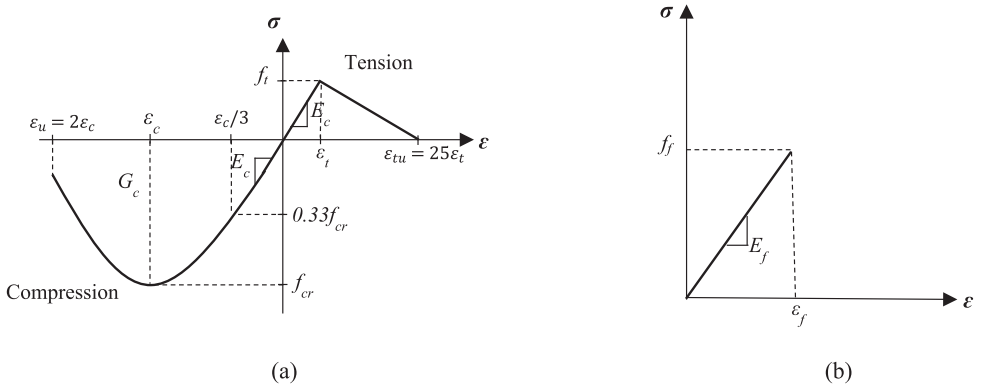

Fig. 7. The stress–strain relationship of (a) mortar [18], and (b) carbon textile [8].

Table 4
Material properties of mortar and textile.

Material	Elastic modulus (GPa)	Poisson ratio	Compressive strength, f_{cr} (MPa)	Tensile strength (MPa)	Fracture energy, G_c (N/mm)
Mortar	35	0.2	47	3.7	0.142
Carbon textile	230	0.3	–	4,500	–

Table 4.

3.2. Boundary conditions and meshing

Based on the experimental analysis, the test specimen was divided into two parts, namely the bond section (short plate) and the anchor section (long plate), with a rectangular cross-section (Fig. 8(a)). The interface between the two plates was the point of the saw cut in the experiment, as shown in Fig. 3. The two plates were connected using the interface element (N6IF) as a discrete crack layer, with zero tension and fracture energy.

The loading was applied at the end of the short plate as a distributed load through displacement-controlled analysis. The boundary conditions were assigned such as to replicate the experimental setup, where the long plate was fixed at one end, whereas at the short plate, the nodes were restrained in all directions except at the direction of the load, as shown in Fig. 8(a). All the nodes of the shorter plate were tied to the centre node of the loaded surface. The finite element model was meshed with an element size of 4 mm (Fig. 8(b)) to obtain sufficient intersection points at the textile mortar interface, as well as appropriate bond stress along the textile.

To determine the suitable mesh size to obtain an accurate FE solution at an ideal computational time, a mesh convergence study was implemented. In this study, five mesh sizes were investigated, namely 10 mm,

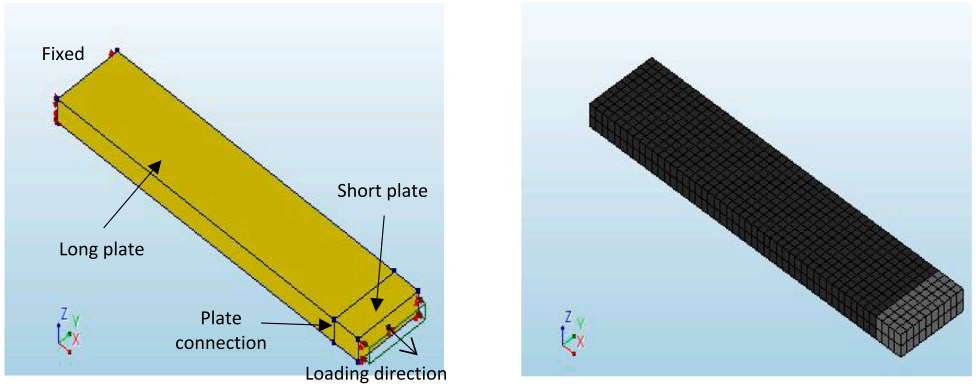

Fig. 8. Overview of 3D model, (a) with boundary conditions and (b) element mesh.

8 mm, 6 mm, 4 mm, and 2 mm corresponding to 131, 397, 673, 1021, and 18,901 elements respectively. The result of FEA was compared for the 20 mm and 60 mm bond lengths, incorporating the five different mesh sizes, with the results shown in Fig. 9. It was observed that the 2 mm and 4 mm mesh sizes resulted in convergence towards experimental data with percentage differences ranging from 1 to 5 %. Considering the computational time, the 4 mm mesh size was taken and used throughout the analysis for other bond lengths.

3.3. Bond slip curve at the interface

A tri-linear bond-slip law [7] was adopted to assign the interface delamination process between materials to reproduce the experimental results, as shown in Fig. 10. This bond-slip model was adopted as it is the closest resemblance to the actual behaviour based on the experimental results. The pullout of fibre for all the bond lengths was identical at the three stages of failure, where the pull-out load was linear initially, followed by a damage descending branch along with fibre pullout due to loss of friction.

In the numerical modelling, a user-defined multilinear bond-slip curve was used to model the interfacial bond-slip response. Furthermore, the normal (K_{nn}) and shear stiffness modulus (K_{tt}) were assigned to the bond-slip interface. The stiffnesses can be calculated using the elastic modulus and shear modulus of mortar, given in Eqs. (1) and (2).

$$K_{nn} = \frac{E_c}{t_i} \tag{1}$$

$$K_{tt} = \frac{G}{t_i} \tag{2}$$

where E_c and G are the elastic and shear modulus of mortar, $G = \frac{E_c}{(1+\upsilon)}$, υ is the Poisson's ratio of mortar, 0.2, and t_i is the assumed thickness of the interface.

Further, in multi-linear curve the debonding failure was considered in three stages, elastic (stage I) up to peak stress at (u_{max}, τ_{max}), followed by descending damage evolution phase (stage II) down to (u_o, τ_o) and finally friction phase (stage III) with horizontal branch until complete debonding (see Fig. 10). The shear stress in the elastic phase will be acting tangential at the textile mortar interface, where the textile displacement will be negligible and shear stress will be linearly increasing. After reaching the peak load, the damage phase initiates at the interface ($\tau = \tau_{max}$). In this phase, the shear stress was affected by slip, so a damaged vector will be used to determine non-linear stresses.

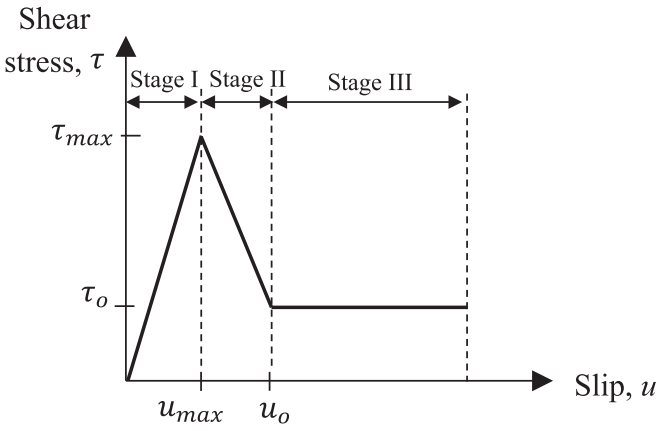

Fig. 10. Tri-linear bond-slip model.

Finally, in stage III, the shear stress becomes constant and can be calculated by the ratio of residual shear strength and maximum bond strength. The bond stress in different phases can be evaluated from Eqs. (3)–(6).

Elastic stage (I)

In this phase, the fibre displacement u was considered from zero to displacement at the peak, u_{max}. The shear stress can be calculated by Eq. (3).

$$\tau(u) = k_1 u \tag{3}$$

where, k_1 is the ratio of maximum stress to peak load displacement. The equation can be written as in Eq. (4).

$$\tau(u) = \frac{\tau_{max}}{u_{max}} . u \quad for \ 0 \le u \le u_{max} \tag{4}$$

Damage evolution stage (II)

In this phase, the fibre displacement u was considered from u_{max} to u_o. A damage variable factor will be used to determine the non-linear shear stress. The curve was plotted with respect to ascending and descending bond stiffness. In both stages, the material interface remains in a cohesive state. The shear stress in stage II can be calculated by Eq. (5).

$$\tau(u) = \frac{k_2(u - u_{max}) + \tau_0(u_o - u)}{u_o - u_{max}} \quad for \quad u_{max} \le u \le u_0 \tag{5}$$

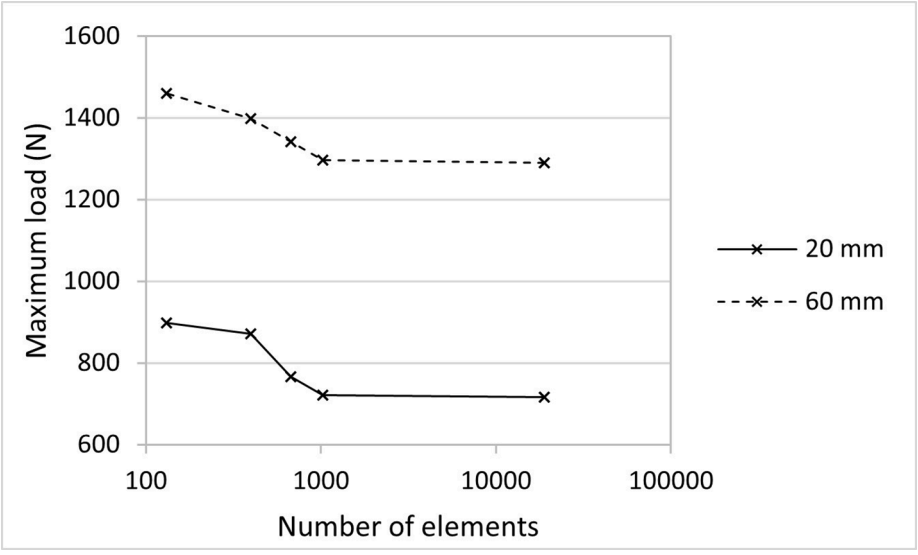

Fig. 9. Convergence analysis for maximum load versus number of elements for 20 mm and 60 mm bond lengths.

where, k_2 is the ratio of residual shear strength, τ_0, and bond strength, τ_{max}.

Friction stage (III)

In this phase, the fibre displacement u was greater than u_o. The shear stress becomes constant and was called residual shear strength. The shear stress in stage III can be calculated using Eq. (6).

$$\tau(u) = k_2\tau_{max} \quad for \quad u \geq u_o \tag{6}$$

3.3.1. Bond slip curves from experimental data

To evaluate the interface shear behaviour of the textile, pullout results from the experiment were used. Initially, the maximum and frictional shear stresses were calculated for the pullout loads, using direct bond stress relation based on textile diameter and the bond length. Then, the shear stress-slip curves were plotted using Eqs. (3)–(6) for different bond lengths.

The evaluated shear stress and slip results were tabulated in Table 5. From the results, it was noticed that with the increase in bond length, the shear stress, τ_{max}, decreases. It was generally observed that the shear stress at the friction phase (τ_o) decreases with increasing bond length, except for the 40 mm bond length. This value varies due to the larger area of circumferential shear stress around fibre, which tends to delay the damage phase.

3.4. Numerical results validation

Non-linear finite element (FE) analysis was performed to obtain the bond-slip behaviour at the textile-mortar interface. The numerical results were compared with experimental pullout load curves, and the results are shown in Fig. 11. In general, the finite element model considering the tri-linear bond-slip model was able to simulate the experimental result with high accuracy. For all the bond lengths, the FE prediction for stage I matches well with the experimental result with a slight difference observed as the load increased. This is because the bond-slip law used in the FE model considers linear-elastic behaviour for stage I, which is slightly different from the damage stage observed in Fig. 4. In stage II for the 20 mm bond length, the FE simulation shows good agreement with the experimental result. However, for stage III, the experimental result shows a curvilinear drop in descending phase (Fig. 11(a)), whereas the FE shows a constant pullout load after 0.3 mm displacement. Stage III results can be improved by using exponential functions in bond slip laws. Similarly, linear behaviour was noticed in stage I for the 30 mm bond length, however, beyond peak load, the fibre displacement was delayed, causing a prolonged pullout curve, due to the fibre resistance against the tangential shear which was not observed in other samples (see Fig. 11(b)).

For 40 mm and 50 mm bond lengths, the load–displacement curves obtained from FE analysis were comparatively better than shorter bond lengths (i.e., 20 mm and 30 mm). However, the difference noted for 50 mm curves was a sudden drop in pullout capacity post-peak (Fig. 11(d)) due to rupture failure, as opposed to pullout failure in 40 mm plates (Fig. 11(c)). Also, the FE results for 40 mm and 50 mm bond lengths were observed to be non-linear beyond 400 N in ascending phase (stage I). This effect can be overcome by considering two sub-stages in stage II bond-slip law which include the initial and rigid body motion stages. Finally, when 60 mm results were compared to all of the bond lengths, a sudden drop in experimental results was noticed in stage II due to the rupture failure of the textile (Fig. 11(e)). Compared to the numerical modelling, the textile was considered to be linearly elastic throughout the debonding process causing the failure to be due to the complete debonding of the textile.

Table 5
Calculated shear stresses and respective slips from experimental data.

Bond length (mm)	Peak load, P_{max} (N)	Shear stress at peak load, τ_{max} (MPa)	Slip at peak, u_{max} (mm)	Load at friction phase, P_o (N)	Shear stress at friction phase, τ_o (MPa)	Slip at friction phase, u_0 (mm)
20	724	10.85	0.28	201	3.02	0.33
30	876	8.77	0.16	187	1.86	2.38
40	926	6.95	0.42	176	1.32	0.95
50	1126	6.75	0.55	308	1.85	0.73
60	1305	6.52	0.80	179	0.89	1.06

The shear traction evolution for 20 mm bond length at different load steps with relative slips of 0.1 mm, 0.3 mm, and 0.35 mm are shown in Fig. 12. Initially, at 0.1 mm traction, shear stress increases linearly with slip and the stress was maximum on the shorter side, whereas minimum stress was recorded at the other end. Further, at 0.3 mm the stress was maximum at the lower tip of the notch on the shorter side. This phenomenon was due to the interfacial shear stress reaching its maximum limit, which led to damage evolution at the textile-mortar interface. Finally, at load step 0.35 mm, the friction phase was initiated at the interface. In this phase, the stress transfers towards the longer part of the plate which leads to the complete debonding of the textile. Similarly, the FE analysis was performed for all the bond lengths and the recorded shear stress is shown in Table 6. For 50 mm and 60 mm bond length specimens, it was evident experimentally that the mode of failure is due to rupture, however, this failure mode is not captured in the numerical modelling. The differences between the FE analysis and experimental results were up to 2 % for the shear stress at peak load (τ_{max}), while for the slip at peak load (u_{max}), the differences were between 4 and 31 %, with the largest difference in the 30 mm bond length.

3.4.1. Failure mode comparison

In this section, the experimental and numerical failure modes of pullout specimens were compared based on the comprehensive results obtained. From the experimental observations of 20 mm bond length specimens, micro cracks were developed at the notch neck when the specimens were loaded beyond 30 percent of maximum load. This phenomenon resembles the change of state from elastic to damage initiation, where the shear stress relatively increases with slip. Upon further loading, the micro-cracks started to widen and the fibre started to yield when the specimen reached its peak load. In the numerical simulation, constant fibre slip was observed with uniform shear stress on the short plate up to the maximum load. The interface failure can be observed at the end of the fibre on the short plate in the FE analysis.

Beyond peak load, the shear stresses induced at the interface drop which leads to sliding of fibre from the matrix. This phenomenon was noticed externally from the experiment, while the interface failure pattern was recorded in FE analysis, as shown in Fig. 12(c). In the analysis, the shear stresses tend to slide towards the long plate and the fibre started delaminating from the matrix with rigid body motion. For the 30 mm and 40 mm bond length specimens, a similar failure pattern alike 20 mm was observed throughout the finite element analysis. The shorter bond length samples failed due to the pullout of textile from the matrix, similar to the experiment.

In the 50 mm and 60 mm bond lengths, the textile bond interface was more rigid compared with the shorter bond lengths. From the experimental testing, it was observed that the formation of microcracks was delayed due to restraining shear stresses around the larger surface area of the textile. Soon after reaching the maximum load, the microcracks initiated and the failure was instantaneous before the crack widening. This led to rupture failure of the textile in both cases. However, in the FE analysis, complete debonding was observed.

4. Conclusions

This article investigates the bond-slip phenomena at the textile-mortar interface through experimental and numerical analyses. The pullout response of textile concrete reinforced with carbon mesh was

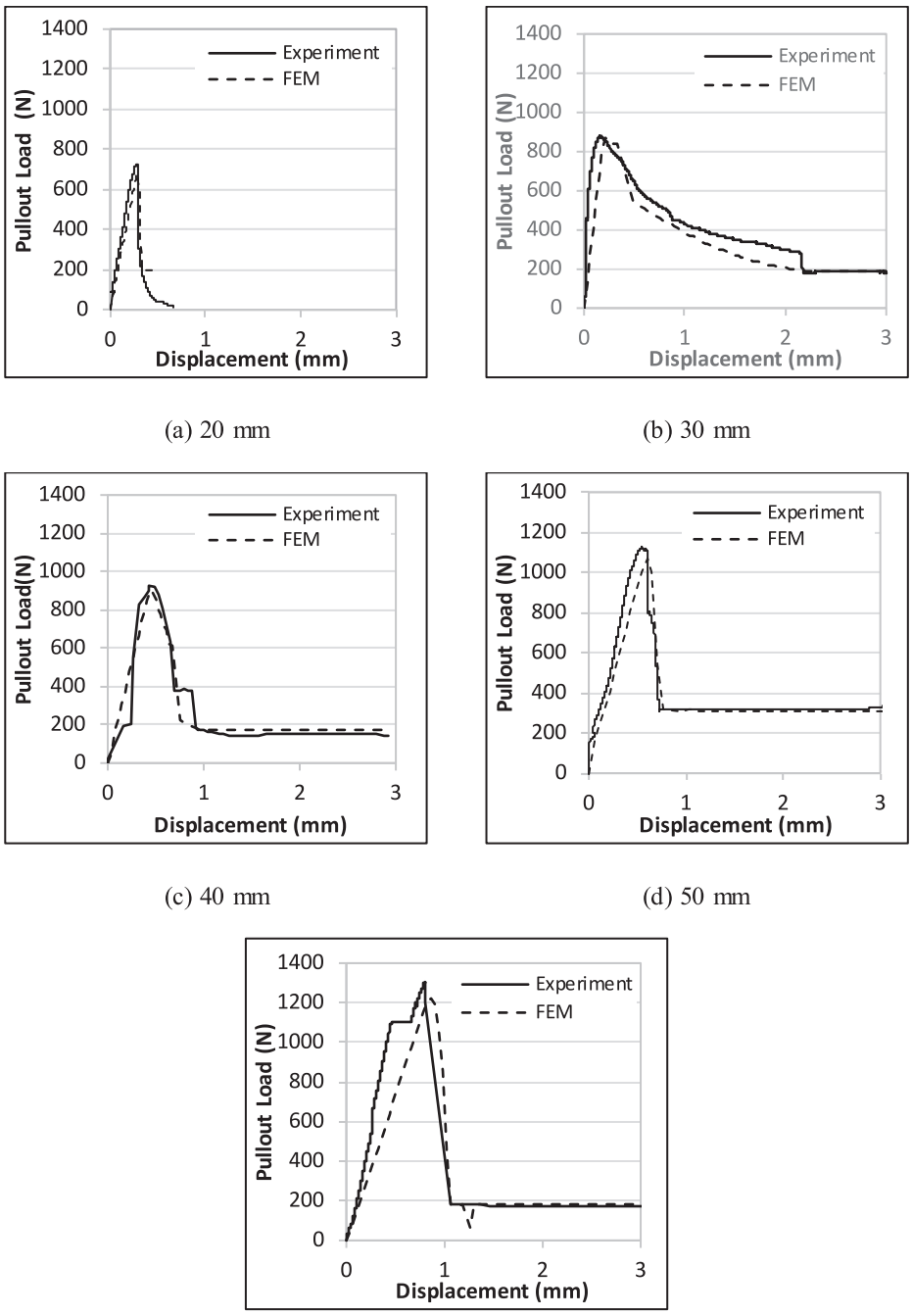

Fig. 11. Comparison of pullout load vs displacement curves for (a) 20 mm (b) 30 mm (c) 40 mm (d) 50 mm, and (e) 60 mm bond lengths.

determined using double-sided pullout tests with symmetrical clamping lengths. Additionally, the general fibre pullout phenomenon curve was used to explain the debonding process. A trilinear bond-slip model was used to calibrate the pullout curves and predict the bond-slip behaviour numerically. The developed numerical model was able to reproduce the experimental results, including maximum load, post-peak behaviour and interfacial slip. From the experimental and numerical results, the following conclusions can be made.

- The maximum pullout loads recorded for 20 mm, 30 mm, 40 mm, 50 mm, and 60 mm bond lengths were 724 N, 876 N, 926 N, 1126 N, and 1305 N respectively.
- The elastic, damage, and debonding phases were identified in the experimental curves. The elastic phase was identified through the uncracked sample at the notch, followed by the damage phase with the initiation of microcracks, and lastly the fibre debonding phase with crack widening. The peak load and fibre slip were directly proportional to the bond length, as the larger surface area surrounding the textile tends to transfer the shear stress to the concrete.
- The shorter bond length specimens (up to 40 mm) showcased a prolonged damage phase after reaching peak strength, due to pullout failure of the fibre. Comparatively, samples with longer bond lengths (50 mm and 60 mm) experienced an instantaneous drop in load after reaching the maximum capacity, due to rupture of fibre.

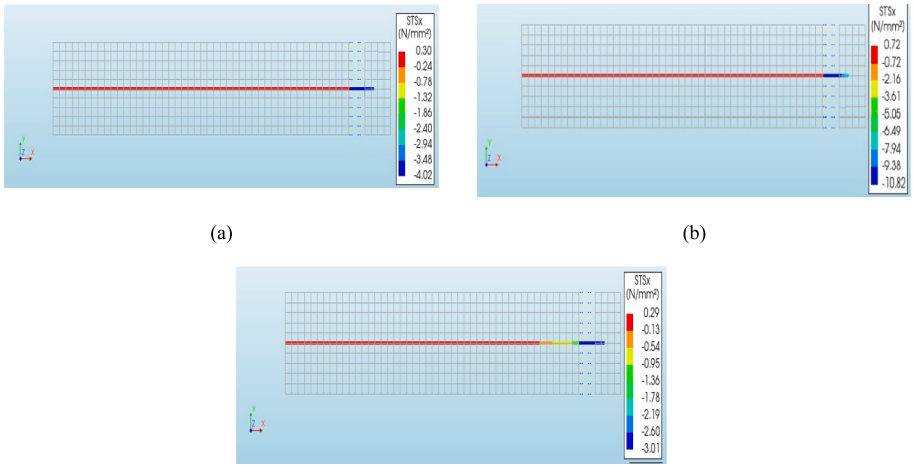

Fig. 12. Shear traction evolution for 20 mm bond length at different load steps with relative slips of (a) 0.10 mm, (b) 0.30 mm, and (c) 0.35 mm.

Table 6
Finite element analysis results of shear traction and slip for different bond lengths.

Bond length (mm)	Shear stress at peak load, τ_{max} (MPa)	Slip at peak load, u_{max} (mm)	Traction stress at friction phase, τ_o (MPa)	Slip at friction phase, u_0 (mm)
20	10.82	0.30	3.01	0.35
30	8.70	0.21	1.86	2.40
40	6.80	0.44	1.31	0.96
50	6.73	0.60	1.85	0.76
60	6.50	0.87	0.89	1.07

- A calibrated trilinear bond-slip relation was adopted to simulate the interfacial response of fibre with elastic, damage, and frictional stages. Using the bond-slip relation, a non-linear finite element analysis was performed to explain the de-bonding process and was compared with the experimental results.
- A similar pullout response was recorded in the finite element analysis for all the bond lengths in the initial elastic phase compared to the experimental results. For specimens with 50 mm and 60 mm bond lengths, a sudden drop was noticed in the experimental results compared to the FE modelling due to fibre rupture. Despite minor differences observed between the experimental and finite element results, the overall performance remained within an acceptable range of below 2 %.

Declaration of Competing Interest

The authors declare that they have no known competing financial interests or personal relationships that could have appeared to influence the work reported in this paper.

Acknowledgements

The authors would like to thank *Kementerian Pendidikan Tinggi Malaysia* for the financial support of this research work under the Fundamental Research Grant Scheme, FRGS/1/2018/TK01/UPM/02/3.

References

[1] AC434. Acceptance criteria for masonry and concrete strengthening using fiber-reinforced cementitious matrix (FRCM) composite systems; 2011.
[2] ASTM C230/C230M-08. Standard specification for flow table for use in tests of hydraulic cement; 2008.
[3] Banholzer B. Bond of a strand in a cementitious matrix. Mater Struct/Mater Constr 2006;39(294):1015–28. https://doi.org/10.1617/s11527-006-9115-y.
[4] Brameshuber W. Recommendation of RILEM TC 232-TDT: test methods and design of textile reinforced concrete. Mater Struct 2016;49(12):4923–7. https://doi.org/10.1617/s11527-016-0839-z.
[5] BS EN 1015-11. BSI Standards Publication Methods of test for mortar for masonry; 2019.
[6] Cai S, Lin J, Fan K, Chen Y, Wang Z. Study on The bonding performance between basalt textile and concrete under freeze-thaw cycles. Eng Fail Anal 2023;146 (October 2022). https://doi.org/10.1016/j.engfailanal.2023.107095.
[7] Carozzi FG, Colombi P, Fava G, Poggi C. A cohesive interface crack model for the matrix – textile debonding in FRCM composites. Compos Struct 2016;143:230–41. https://doi.org/10.1016/j.compstruct.2016.02.019.
[8] Contamine R, Si-Larbi A, Than NQ, Hamelin P. Numerical modeling of reinforced concrete beams under shear stress with and without external textile-reinforced concrete reinforcement. J Reinf Plast Compos 2011;30(15):1293–303. https://doi.org/10.1177/0731684411420189.
[9] Gómez J, Torres L, Barris C. Characterization and simulation of the bond response of NSM FRP reinforcement in Concrete. Materials 2020;13(7). https://doi.org/10.3390/MA13071770.
[10] Jiang J, Jiang C, Li B, Feng P. Bond behavior of basalt textile meshes in ultra-high ductility cementitious composites. Compos B Eng 2019;174(June). https://doi.org/10.1016/j.compositesb.2019.107022.
[11] Kong K, Mesticou Z, Michel M, Si Larbi A, Junes A. Comparative characterization of the durability behaviour of textile-reinforced concrete (TRC) under tension and bending. Compos Struct 2017;179:107–23. https://doi.org/10.1016/j.compstruct.2017.07.030.
[12] Krüger, M. Vorgespannter Textilbewehrter Beton (Issue July 2004); 2004.
[13] Li Q, Xu S. Experimental research on mechanical performance of hybrid fiber reinforced cementitious composites with polyvinyl alcohol short fiber and carbon textile. J Compos Mater 2011;45(1):5–28. https://doi.org/10.1177/0021998310371529.
[14] Liu S, Rawat P, Chen Z, Guo S, Shi C, Zhu D. Pullout behaviors of single yarn and textile in cement matrix at elevated temperatures with varying loading speeds. Compos B Eng 2020;199(December 2019). https://doi.org/10.1016/j.compositesb.2020.108251.
[15] Lorenz E, Ortlepp R. Bond behavior of textile reinforcements - development of a pull-out test and modeling of the respective bond versus slip relation. RILEM Bookseries 2011;(June):479–86. https://doi.org/10.1007/978-94-007-2436-5.
[16] Lorenz E, Schütze E, Schladitz F, Curbach M. Textilbeton - Grundlegende Untersuchungen im Überblick. Beton- Stahlbetonbau 2013;108(10):711–22. https://doi.org/10.1002/best.201300041.
[17] Mehdikhani M, Gorbatikh L, Verpoest I, Lomov SV. Voids in fiber-reinforced polymer composites: a review on their formation, characteristics, and effects on mechanical performance. J Compos Mater 2019;53(12):1579–669. https://doi.org/10.1177/0021998318772152.
[18] Nabilah AB, Koh CG, Izian AK, Abd Aziz FNA. Development of finite element analysis for intermediate length coupling beams considering bond-slip interface. Int J Concr Struct Mater 2020;14(1):33. https://doi.org/10.1186/s40069-020-00409-w.
[19] Rampini MC, Zani G, Colombo M, di Prisco M. Mechanical behaviour of TRC composites: Experimental and analytical approaches. Applied Sciences (Switzerland) 2019;9(7). https://doi.org/10.3390/app9071492.
[20] Scheerer S, Schladitz F, Curbach M. Textile reinforced concrete - from the idea to a high performance material. In: 11th International Symposium on Ferrocement and Textile Reinforced Concrete 3rd ICTRC; 2015. p. 15–34.
[21] Scholzen A, Chudoba R, Hegger J. Thin-walled shell structures made of textile-reinforced concrete: Part II: Experimental characterization, ultimate limit state

assessment and numerical simulation. Struct Concr 2015;16(1):115–24. https://doi.org/10.1002/suco.201400046.
[22] Sciegaj A, Larsson F, Lundgren K. Experiments and calibration of a bond-slip relation and efficiency factors for textile reinforcement in concrete. Cem Concr Compos 2022;134(August):104756. https://doi.org/10.1016/j.cemconcomp.2022.104756.
[23] Shiping Y, Boxue W, Chenxue Z, Shuang L. Bond performance between textile reinforced concrete (TRC) and brick masonry under conventional environment. Structures 2022;36(December 2021):392–403. https://doi.org/10.1016/j.istruc.2021.12.029.
[24] Sueki S, Soranakom C, Mobasher B, Peled A. Pullout-slip response of fabrics embedded in a cement paste matrix. J Mater Civ Eng 2007;19(9):718–27. https://doi.org/10.1061/(ASCE)0899-1561(2007)19:9(718).
[25] Venigalla SG, Nabilah AB, Mohd Nasir NA, Safiee NA, Abd Aziz FNA. Textile-reinforced concrete as a structural member: a review. Buildings 2022;12(4):474. https://doi.org/10.3390/buildings12040474.
[26] Wang L, Yin S, Wang F. Interfacial bonding performance of textile reinforced ECC and seawater sea-sand concrete under a dry-wet environment. Constr Build Mater 2023;368(October 2022). https://doi.org/10.1016/j.conbuildmat.2023.130384.
[27] Williams Portal N, Fernandez Perez I, Nyholm Thrane L, Lundgren K. Pull-out of textile reinforcement in concrete. Constr Build Mater 2014;71:63–71. https://doi.org/10.1016/j.conbuildmat.2014.08.014.
[28] Yin S, Wang B, Wang F, Xu S. Bond investigation of hybrid textile with self-compacting fine-grain concrete. J Ind Text 2017;46(8):1616–32. https://doi.org/10.1177/1528083716629137.
[29] Zhang XB, Aljewifi H, Li J. Failure behaviour investigation of continuous yarn reinforced cementitious composites. Constr Build Mater 2013;47:456–64. https://doi.org/10.1016/j.conbuildmat.2013.05.022.
[30] Zhu M, Zhu JH, Ueda T, Matsumoto K, Su M. Bond behavior of carbon fabric reinforced cementitious matrix (FRCM) composites considering matrix impregnation. Compos Struct 2021;262(November 2020). https://doi.org/10.1016/j.compstruct.2020.113350.